Correlated conformational events in EF-G and the ribosome regulate translocation

James B. Munro, Michael R. Wasserman, Roger B. Altman, Leyi Wang & Scott C. Blanchard

SUPPLEMENTARY INFORMATION

SUPPLEMENTARY FIGURES

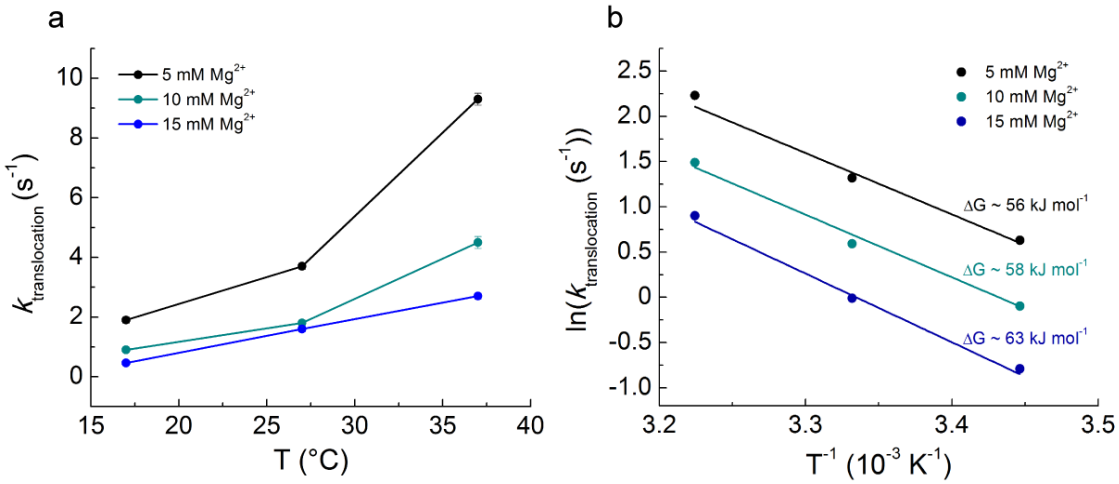

Supplementary Figure 1. Kinetics of translocation across a range of conditions. Translocation was measured in bulk with a fluorescence-based assay monitoring pyrene-labeled mRNA fluorescence as a function of time[4]. Data was acquired across a range of temperatures (17 °C, 27 °C and 37 °C) and Mg^{2+} concentrations (5 mM, 10 mM and 15 mM). (a) The dependence of translocation rate on temperature and Mg^{2+} concentration for pre-translocation complexes containing A-site $tRNA^{fMet}$ and P-site fMet-Phe-$tRNA^{Phe}$. (b) Arrhenius plots compiled from the same data. The slopes of the linear fits report on the apparent activation energies for translocation. Data are presented as the mean ± standard error from at least three independent measurements.

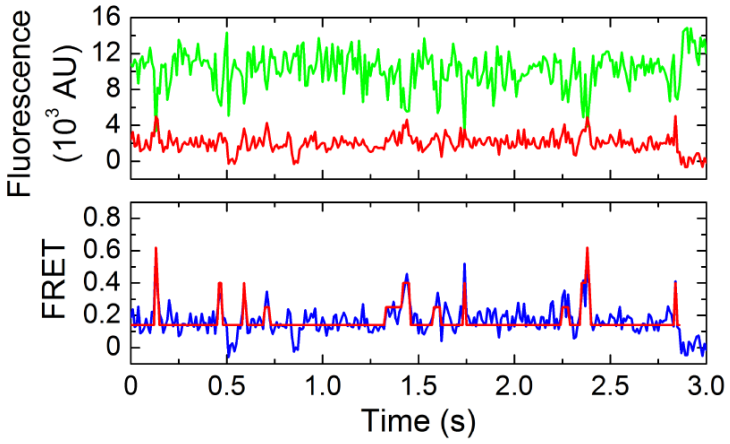

Supplementary Figure 2. Dynamics of the pre-translocation complex. Prior to the addition of EF-G pre-translocation complexes with labeled P-site tRNA and L1 display transitions between four FRET states. (Top) Single-molecule fluorescence (Cy3, green; Cy5, red), and (bottom) FRET (blue) trajectories. Overlaid in red is the idealization generated during HMM analysis with the model shown in **Supplementary Figure 4a**.

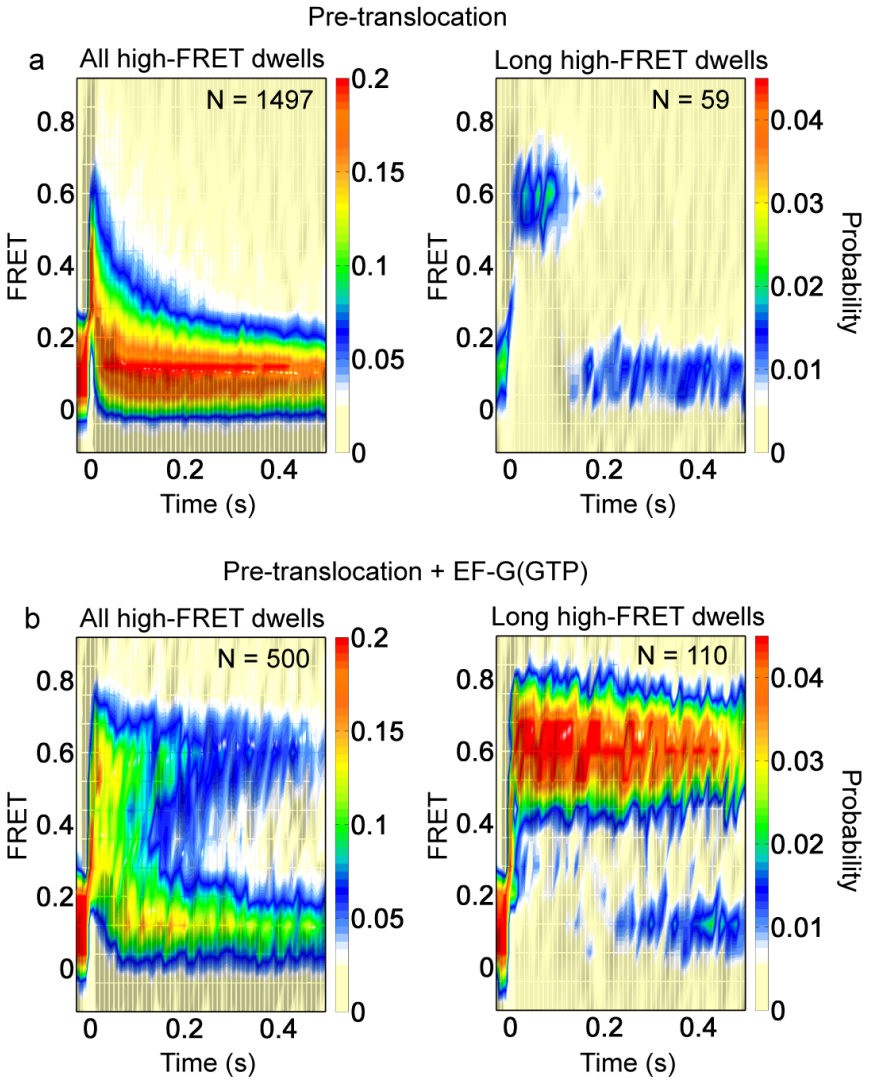

Supplementary Figure 3. Contour plots of L1-tRNA FRET trajectories. smFRET trajectories acquired during delivery of EF-G(GTP) to complexes containing labeled P-site tRNA and L1, such as those shown in **Figure 2a**, were compiled into two-dimensional histograms. (Left column) All transitions to high FRET were post-synchronized, or (right column) only long-lived (>200 ms) dwells in high FRET were post-synchronized for trajectories from (a) pre-translocation complexes, and (b) following the addition of EF-G(GTP).

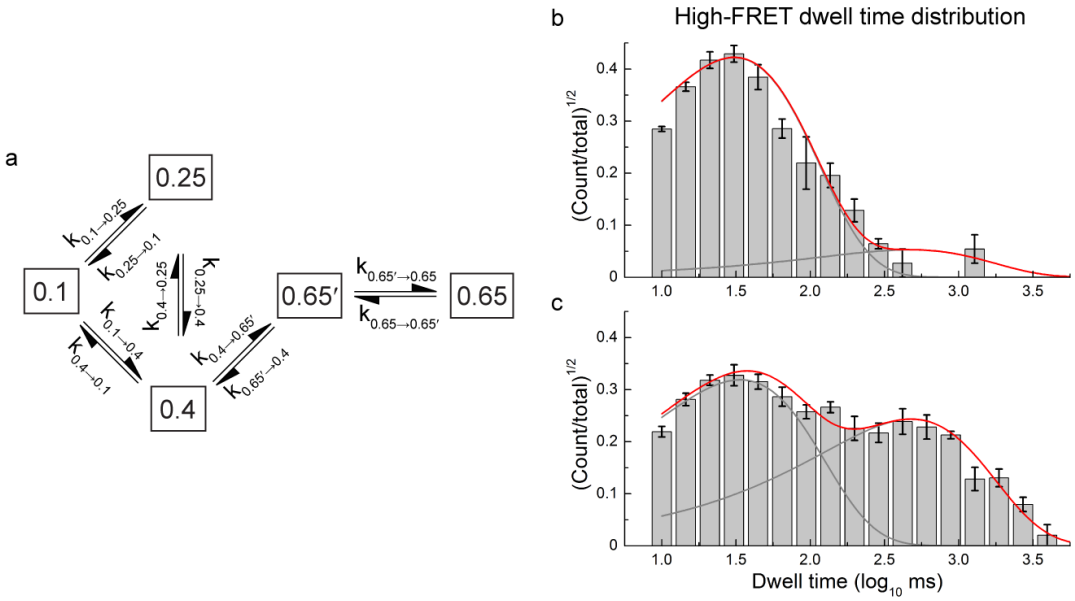

Supplementary Figure 4. Hidden Markov modeling of L1-tRNA FRET trajectories. smFRET trajectories acquired from ribosome complexes containing labeled P-site tRNA and L1 were idealized to the Markov chain model with four FRET states shown in (a). (b) Prior to addition of EF-G(GTP) the distribution of dwell times in the high-FRET state (0.65′) was well fit with a single rate constant. (c) During addition of EF-G(GTP) a long-lived component in the high-FRET state dwell time distribution emerged (0.65). Overlaid on the histograms are the fits obtained through maximum likelihood optimization in QuB[2]. Error bars represent the standard deviation from three independent data sets.

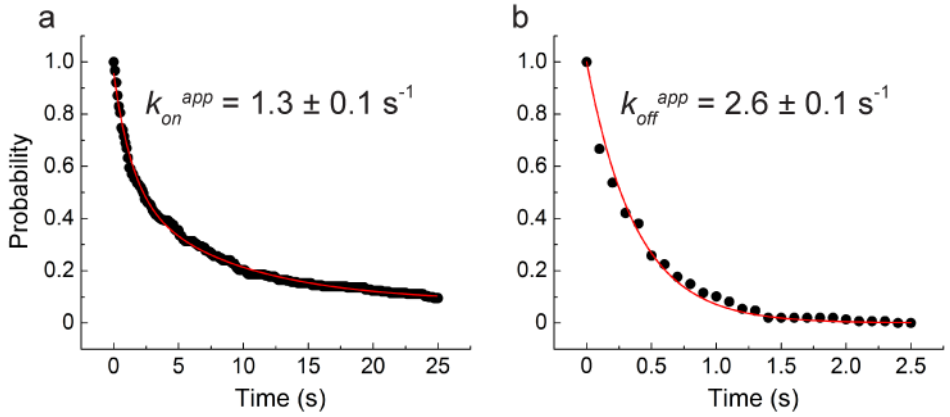

Supplementary Figure 5. Kinetic analysis of EF-G-tRNA FRET trajectories. The smFRET trajectories obtained during the delivery of fluorescently labeled EF-G to pre-translocation complexes with labeled A-site tRNA were analyzed by manually placing a threshold at 0.3 FRET. The resulting dwell times that fell above or below this threshold were compiled into histograms and fit to exponential functions (R^2 ≈ 0.99). (a) The distribution of times leading to formation of the observed FRET event was fit to a double exponential with the dominant (~70%) rate constant shown, and a minor rate constant of 0.16 ± 0.01 s^{-1}. (b) The distribution of the dwell times of the observed FRET event was well fit by a single exponential with the rate constant shown. Error bars represent the standard error.

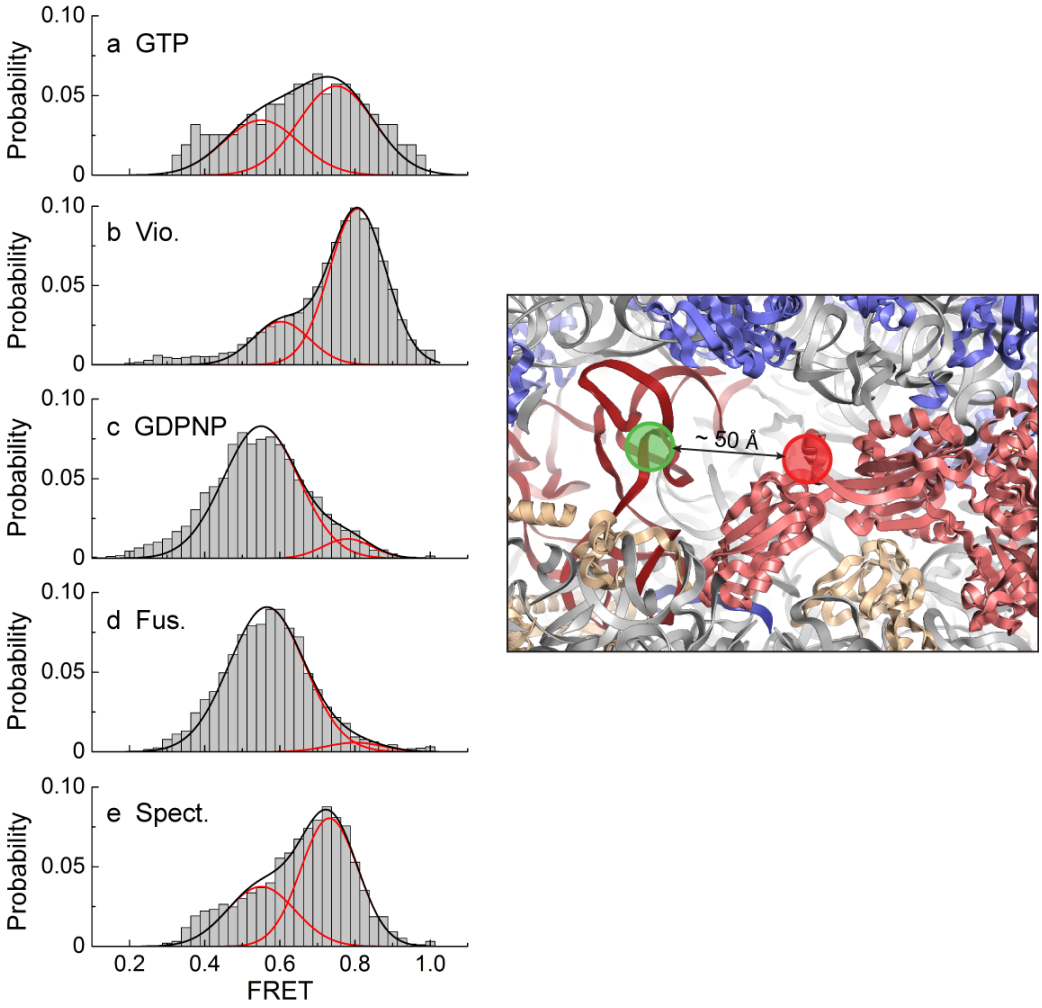

Supplementary Figure 6. The distributions in FRET observed between EF-G and the A-site tRNA. The FRET trajectories observed upon delivery of labeled EF-G to pre-translocation complexes with labeled A-site tRNA were idealized to a two-state model in QuB[1] containing a zero- and high (0.65)-FRET state. Only the dwells corresponding to non-zero FRET states were compiled into the histograms shown (left panels). In all panels, the distributions have been fit to the sum of two Gaussian functions with means at 0.75 and 0.55 FRET, and standard deviations between 0.15 and 0.2 ($R^2 \geq 0.92$). (a) In the uninhibited case (GTP), the high-FRET state is predominant, suggestive of EF-G's interaction with the pre-translocation complex. Evidence of the lower-FRET state (~0.55) is also present, consistent with the greater distance between EF-G and the P-site tRNA following translocation (right panel). (b) In the presence of 200 μM viomycin (Vio.) the high-FRET state is more dominant, consistent with inhibition of translocation. (c) When GTP hydrolysis is inhibited with GDPNP, the low-FRET state is dominant, consistent with EF-G remaining on the ribosome for prolonged duration in the post-translocation state. (d) Similarly, in the presence of 50 μM fusidic acid (Fus.) the low-FRET state is dominant. (e) In the presence of 5 mM spectinomycin (Spect.), the high-FRET state is dominant, consistent with inhibition of translocation. (Right panel) Also shown is the crystal structure of the fusidic-acid-stalled post-translocation ribosome complex[5], which predicts an approximate distance of 50 Å between the sites of labeling on the P-site tRNA (red) and EF-G (pink), consistent with the observed 0.55 FRET state.

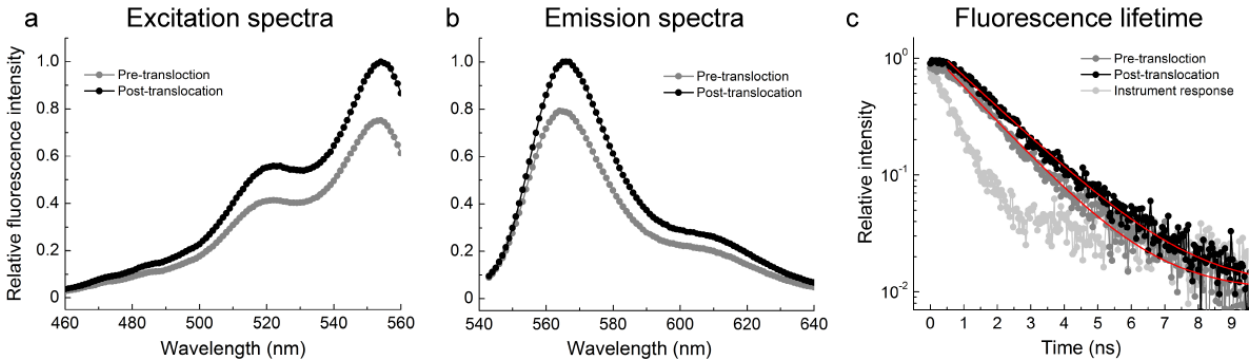

Supplementary Figure 7. Photophysical analysis of Cy3 bound to tRNA^{Phe} before and after translocation. (a) Excitation spectra measured at 550 nm emission, and the (b) emission spectra resulting from excitation at 532 nm for (grey) pre-translocation and (black) post-translocation complexes. The integrated area of the emission spectra increased by approximately 27% following translocation. (c) The fluorescence lifetime measurements, well fit by single exponential functions, indicated a small increase in Cy3 fluorescence lifetime following translocation: 0.877 ± 0.005 ns and 1.041 ± 0.005 ns for pre- and post-translocation complexes, respectively. Error bars represent the standard error from three independent measurements.

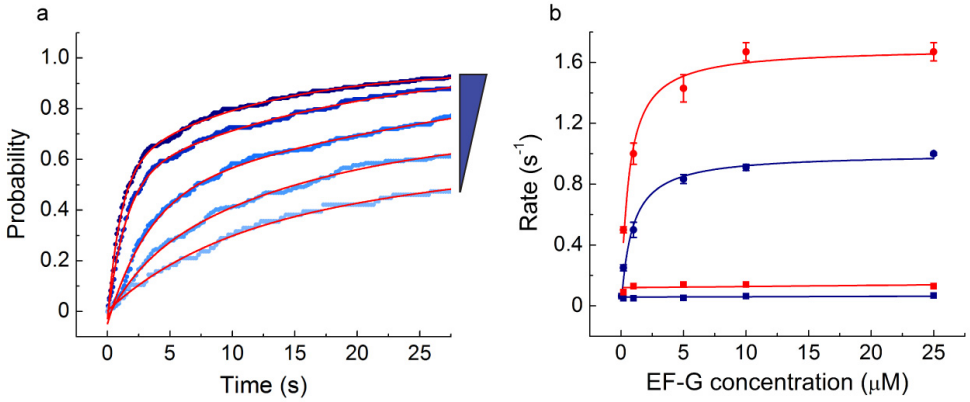

Supplementary Figure 8. The dependence of translocation rate on EF-G concentration. (a) The times until the step-like increase in Cy3 fluorescence observed upon delivery of unlabeled EF-G to pre-translocation complexes with P-site tRNA^{fMet} and labeled A-site fMet-Phe-tRNA^{Phe} were identified manually and compiled into histograms. The resulting distributions were well fit by double exponential functions. The blue triangle indicates increasing EF-G concentration (0.05–25 μM). (b) The fast (circles) and slow (squares) components of the double exponential fits as a function of EF-G concentration for complexes with (blue) P-site tRNA^{fMet} and labeled A-site fMet-Phe-tRNA^{Phe}, and (red) P-site tRNA^{Phe} and labeled A-site NAcPhe-Lys-tRNA^{Lys}. The fast components increased with increasing EF-G concentration, fitting a hyperbola (**Fig. 4**). The slow components remained constant across EF-G concentration. In both cases the slower, EF-G-independent rate constants (~0.07 s^{-1} and ~0.12 s^{-1} for P-site tRNA^{fMet} and tRNA^{Phe} complexes respectively) were at least an order of magnitude faster than expected for spontaneous translocation[6-9]. The amplitude of the fast component increased to approximately 60% and 70% at saturating EF-G concentrations for P-site tRNA^{fMet} and tRNA^{Phe}, respectively. Error bars represent the standard error.

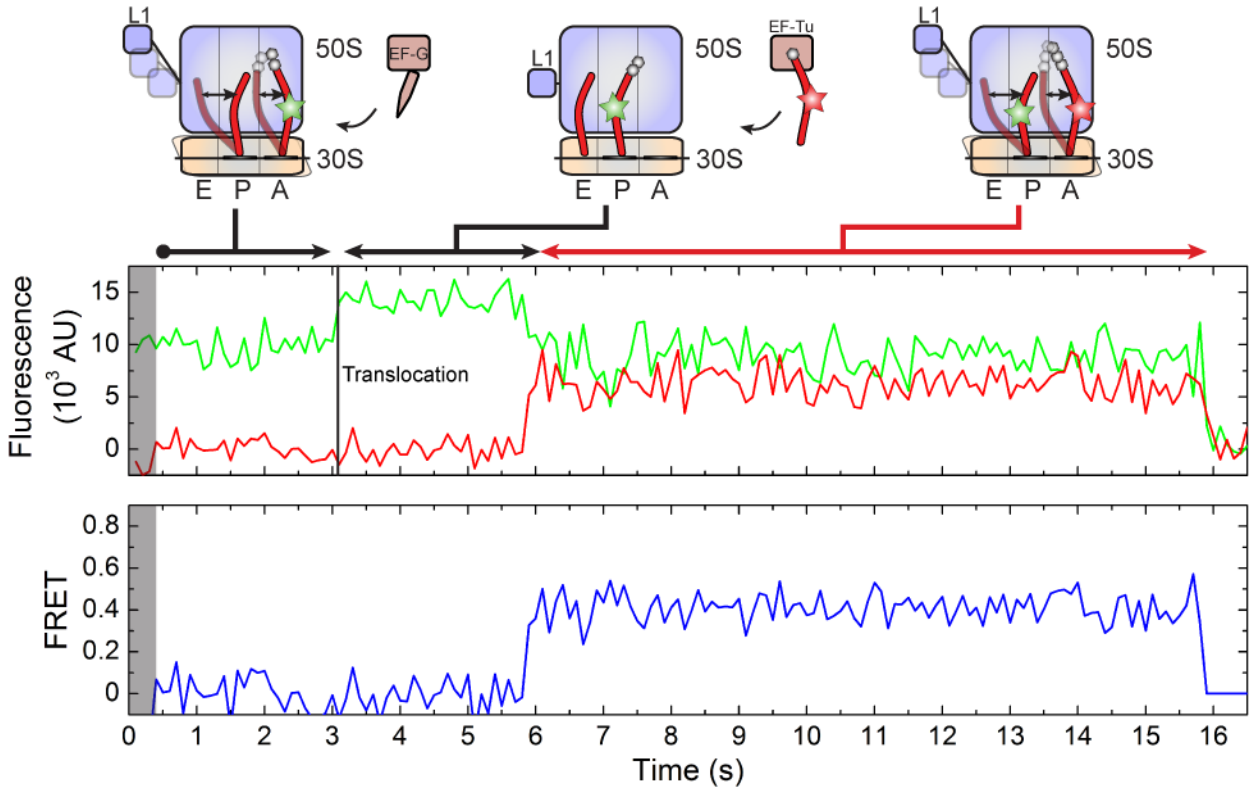

Supplementary Figure 9. The appearance of FRET between P- and A-site tRNAs occurs only after the rise in Cy3 fluorescence intensity. Single-molecule fluorescence (Cy3, green; Cy5, red) and FRET (blue) trajectories obtained by co-injecting 10 μM EF-G(GTP) and 0.02 μM EF-Tu(GTP)-Lys-tRNA^{Lys}(Cy3-acp^{3}U47) to pre-translocation complexes with P-site tRNA^{fMet}. Binding of labeled tRNA^{Lys} occurred only after the step-like increase in Cy3 fluorescence intensity identified as the translocation event. Cartoon models indicate the sites of labeling and the presumed dynamic elements.

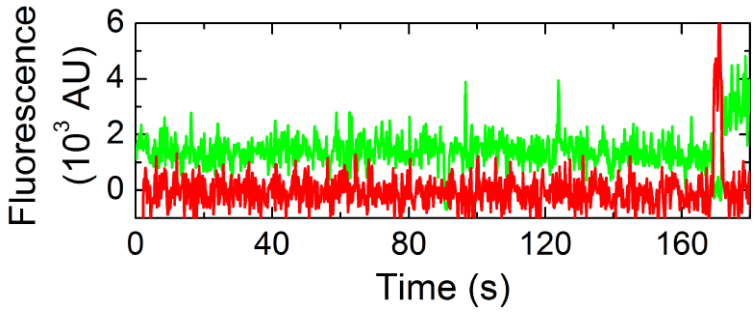

Supplementary Figure 10. Translocation experiments observed with dual Cy3 and Cy5 excitation. Fluorescence trajectories (Cy3, green; Cy5, red) acquired from complexes containing P-site $tRNA^{fMet}$, and A-site fMet-Phe-$tRNA^{Phe}$(Cy3-acp^3U47) in the presence of 20 nM Cy5-EF-G. Data was acquired under conditions in which both Cy3 and Cy5 were directly excited. At the present experimental time resolution (100 ms), no FRET is observed prior to EF-G engaging the A site to mediate translocation.

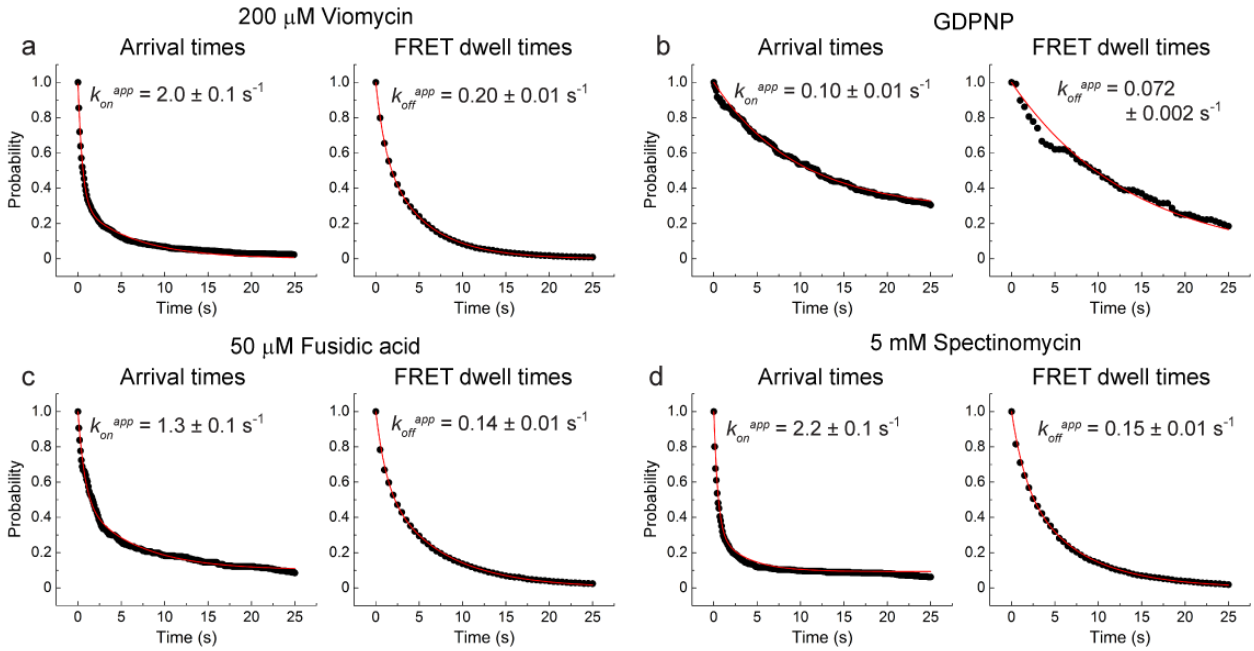

Supplementary Figure 11. Kinetic analysis of EF-G-tRNA FRET signal in the presence of inhibitors. The smFRET trajectories obtained during the delivery of fluorescently labeled EF-G to pre-translocation complexes with labeled A-site tRNA in the presence of (a) viomycin (200 μM), (b) the non-hydrolyzable GTP analogue, GDPNP, (c) fusidic acid (50 μM) or (d) spectinomycin (5 mM) were analyzed by manual thresholding. The resulting dwell times were compiled into histograms. Shown here are the distributions of times leading to the observation of FRET ("Arrival Times"), and the distributions of the lifetimes of the FRET event ("FRET dwell times"). All the distributions were fit to double exponentials ($R^2 \approx 0.99$), with two exceptions—the Arrival times and FRET dwell times observed in the presence of GDPNP were fit to single exponentials ($R^2 \approx 0.96$). For those distributions fit to double exponentials, the rates shown represent the dominant components (~70%). The minor components are as follows: (a, Viomycin) Arrival time: 0.16 ± 0.01, FRET dwell time: 0.93 ± 0.04; (c, Fusidic acid) Arrival time: 0.16 ± 0.01, FRET dwell time: 0.83 ± 0.06; (d, Spectinomycin) Arrival time: 0.29 ± 0.01, FRET dwell time: 0.63 ± 0.06. The Arrival times were determined from data acquired at 100 ms time resolution; the FRET dwell times were determined from data acquired at 500 ms time resolution under conditions in which fluorophore photobleaching was negligible. Error bars represent the standard error.

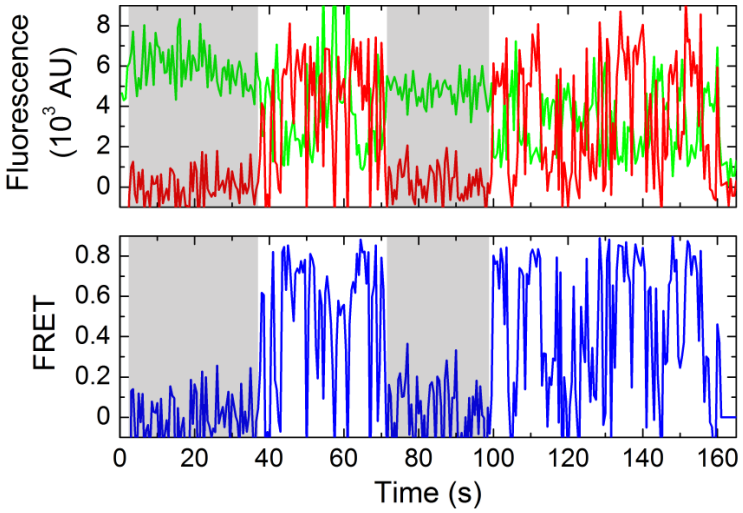

Supplementary Figure 12. Mixed dynamics observed in the presence of viomycin and low concentrations of EF-G. Single-molecule fluorescence (Cy3, green; Cy5, red) and FRET (blue) trajectories acquired from complexes containing P-site $tRNA^{fMet}$, and A-site fMet-Phe-$tRNA^{Phe}$ (Cy3-acp^3U47) in the presence of 20 nM Cy5-EF-G and 0.2 mM viomycin. Direct inspection of the individual FRET trajectories reveal evidence of distinct zero-FRET configurations: short-lived zero-FRET events in the EF-G-bound ribosome and long-lived zero-FRET events, where EF-G is not bound (gray shaded region).

SUPPLEMENTARY TABLES

L1-tRNA FRET Transitions Rates (s^{-1})

P-site tRNA	$k_{0.1\rightarrow0.25}$	$k_{0.1\rightarrow0.4}$	$k_{0.25\rightarrow0.1}$	$k_{0.25\rightarrow0.4}$	$k_{0.4\rightarrow0.1}$
tRNA^{fMet}	0.79 ± 0.03	1.4 ± 0.1	7.3 ± 0.3	8.4 ± 0.3	26 ± 1
tRNA^{fMet}, EF-G(GTP)	1.7 ± 0.1	1.0 ± 0.1	9.9 ± 0.3	6.2 ± 0.3	12 ± 1
tRNA^{fMet}*	1.0 ± 0.1	1.2 ± 0.2	9.3 ± 0.9	14 ± 2	8.6 ± 0.3
tRNA^{fMet}, EF-G(GTP)*	1.4 ± 0.1	1.4 ± 0.1	11 ± 1	12 ± 1	9.0 ± 0.8
tRNA^{Phe}	1.7 ± 0.1	2.6 ± 0.3	6.0 ± 0.9	11 ± 1	17 ± 1
tRNA^{Phe}, EF-G(GTP)	1.7 ± 0.3	2.6 ± 0.3	6.4 ± 0.6	12 ± 1	17 ± 2
tRNA^{Phe}*	1.5 ± 0.2	3.2 ± 0.5	6.9 ± 0.2	15 ± 1	21 ± 3
tRNA^{Phe}, EF-G(GTP)*	1.5 ± 0.1	3.0 ± 0.5	6.4 ± 0.6	16 ± 1	14 ± 1
tRNA^{fMet}, Vio.	1.7 ± 0.2	1.2 ± 0.1	8.5 ± 0.5	9.3 ± 0.5	7.6 ± 0.8
tRNA^{fMet}, Spect.	3.0 ± 0.2	5.4 ± 0.3	7.3 ± 0.2	13 ± 1	20 ± 1
tRNA^{fMet}, Thio.	1.5 ± 0.1	3.8 ± 0.3	10 ± 1	17 ± 1	27 ± 2
	$k_{0.4\rightarrow0.25}$	$k_{0.4\rightarrow0.65'}$	$k_{0.65'\hookrightarrow0.4}$	$k_{0.65'\hookrightarrow0.65}$	$k_{0.65\rightarrow0.65'}$
tRNA^{fMet}	18 ± 1	20 ± 1	46 ± 2	--	--
tRNA^{fMet}, EF-G(GTP)	13 ± 1	23 ± 1	40 ± 3	10 ± 1	2.7 ± 0.2
tRNA^{fMet}*	12 ± 2	11 ± 1	43 ± 2	--	--
tRNA^{fMet}, EF-G(GTP)*	12 ± 2	15 ± 1	40 ± 2	11 ± 1	3.4 ± 0.9
tRNA^{Phe}	23 ± 2	21 ± 1	39 ± 3	--	--
tRNA^{Phe}, EF-G(GTP)	19 ± 1	24 ± 2	31 ± 3	5.7 ± 0.9	3.1 ± 0.3
tRNA^{Phe}*	21 ± 1	28 ± 1	49 ± 5	--	--
tRNA^{Phe}, EF-G(GTP)*	17 ± 1	27 ± 1	42 ± 3	7.8 ± 0.9	8.2 ± 0.9
tRNA^{fMet}, Vio.	12 ± 1	28 ± 2	38 ± 1	--	--
tRNA^{fMet}, Spect.	20 ± 1	35 ± 1	35 ± 1	--	--
tRNA^{fMet}, Thio.	19 ± 1	32 ± 1	40 ± 2	--	--

Supplementary Table 1. Kinetic analysis of smFRET trajectories acquired on complexes with labeled L1 and P-site tRNA. smFRET trajectories were fit to the model shown in **Supplementary Figure 4** by hidden Markov modeling procedures[1-3]. The data acquired in the presence of EF-G(GTP) required two high-FRET states: a short-lived state (0.65′), and a long-lived state (0.65). All data were acquired in the presence of 15 mM Mg^{2+}, except those indicated with a '*', which were acquired with 5 mM Mg^{2+}. The rates are presented as a mean ± standard error determined during maximum likelihood optimization[2].

(a) Rates of unlocked state formation from L1-tRNA FRET experiments (s^{-1})

P-site tRNA	$k_{low\rightarrow}$	$k_{\rightarrow high}$	$k_{high\rightarrow}^{unstable}$	$k_{high\rightarrow}^{stable}$
$tRNA^{fMet}$	2.2 ± 0.2	0.7 ± 0.2	46 ± 2	--
$tRNA^{fMet}$, EF-G(GTP)	2.7 ± 0.2	0.9 ± 0.2	40 ± 3	2.7 ± 0.1
$tRNA^{fMet*}$	2.2 ± 0.3	0.8 ± 0.2	43 ± 2	--
$tRNA^{fMet}$, EF-G(GTP)*	2.8 ± 0.1	1.1 ± 0.1	40 ± 2	3.4 ± 0.9
$tRNA^{Phe}$	3.7 ± 0.3	1.7 ± 0.2	45 ± 2	--
$tRNA^{Phe}$, EF-G(GTP)	4.3 ± 0.3	1.6 ± 0.2	40 ± 3	4.0 ± 0.3
$tRNA^{Phe*}$	4.7 ± 0.7	1.9 ± 0.2	49 ± 5	--
$tRNA^{Phe}$, EF-G(GTP)*	4.5 ± 0.6	2.2 ± 0.3	42 ± 3	8.2 ± 0.9

(b) Rates of translocation from EF-G-tRNA FRET experiments (s^{-1})

P-site tRNA	*EF-G-tRNA FRET*	
	k_{on}^{app}	k_{off}^{app}
$tRNA^{fMet}$, EF-G(GTP)	1.3 ± 0.1	2.6 ± 0.1
$tRNA^{fMet}$, EF-G(GTP)*	1.5 ± 0.1	3.2 ± 0.1
$tRNA^{Phe}$, EF-G(GTP)	1.6 ± 0.1	4.3 ± 0.2
$tRNA^{Phe}$, EF-G(GTP)*	1.7 ± 0.1	8.8 ± 0.4
$tRNA^{fMet}$, EF-G(GTP), Vio.	2.0 ± 0.1	0.20 ± 0.01
$tRNA^{fMet}$, EF-G(GDPNP)	0.10 ± 0.01	0.072 ± 0.002
$tRNA^{fMet}$, EF-G(GTP), Fus.	1.3 ± 0.1	0.14 ± 0.01
$tRNA^{fMet}$, EF-G(GTP), Spect.	2.2 ± 0.1	0.15 ± 0.01

Supplementary Table 2. Apparent transition rates observed in smFRET experiments. (a) Summary of transition rates determined from hidden Markov modeling of smFRET trajectories acquired from L1- and P-site tRNA-labeled pre-translocation complexes. The complete results of this kinetic analysis are shown in **Supplementary Table 1**. Error bars represent the standard error from three independent measurements. (b) The rates of FRET appearance $\left(k_{on}^{app}\right)$ and disappearance $\left(k_{off}^{app}\right)$ for translocation experiments performed with dye-labeled EF-G and A-site tRNA were determined by manual thresholding and dwell-time histogram fitting (**Supplementary Figs. 5** and **11**). All data were acquired in the presence of 15 mM Mg^{2+}, except those indicated with a '*', which were acquired with 5 mM Mg^{2+}. Error bars represent the standard error.

Rates of unlocked state formation from L1-tRNA FRET experiments (s^{-1})

P-site tRNA	$k_{low\rightarrow}$	$k_{\rightarrow high}$	$k_{high\rightarrow}^{unstable}$
$tRNA^{fMet}$	2.2 ± 0.2	0.7 ± 0.2	46 ± 2
$tRNA^{fMet}$, Vio.	3.0 ± 0.3	1.4 ± 0.1	38 ± 1
$tRNA^{Phe}$, Spect.	8.4 ± 0.3	3.4 ± 0.2	35 ± 1
$tRNA^{Phe}$, Thio.	5.3 ± 0.3	2.0 ± 0.1	40 ± 2

Supplementary Table 3. Rates of unlocked state formation in the presence of translocation inhibitors. The rate of unlocked state formation was determined for pre-translocation complexes containing deacylated $tRNA^{fMet}$ in the P site. The rates were calculated from those reported in **Supplementary Table 2**. The rates are presented as a mean ± standard error determined from three independent data sets[2].

SUPPLEMENTARY REFERENCES

1. Qin, F. Restoration of single-channel currents using the segmental k-means method based on hidden Markov modeling. *Biophys J* **86**, 1488-501 (2004).
2. Qin, F., Auerbach, A. & Sachs, F. Estimating single-channel kinetic parameters from idealized patch-clamp data containing missed events. *Biophys J* **70**, 264-280 (1996).
3. Munro, J.B. et al. Spontaneous formation of the unlocked state of the ribosome is a multistep process. *Proc Natl Acad Sci U S A* **107**, 709-14 (2010).
4. Studer, S.M., Feinberg, J.S. & Joseph, S. Rapid kinetic analysis of EF-G-dependent mRNA translocation in the ribosome. *J Mol Biol* **327**, 369-81 (2003).
5. Gao, Y.G. et al. The structure of the ribosome with elongation factor G trapped in the posttranslocational state. *Science* **326**, 694-9 (2009).
6. Fredrick, K. & Noller, H. Catalysis of ribosomal translocation by sparsomycin. *Science* **300**, 1159-1162 (2003).
7. Cukras, A.R., Southworth, D.R., Brunelle, J.L., Culver, G.M. & Green, R. Ribosomal proteins S12 and S13 function as control elements for translocation of the mRNA:tRNA complex. *Mol Cell* **12**, 321-8 (2003).
8. Gavrilova, L.P., Kostiashkina, O.E., Koteliansky, V.E., Rutkevitch, N.M. & Spirin, A.S. Factor-free ("non-enzymic") and factor-dependent systems of translation of polyuridylic acid by Escherichia coli ribosomes. *J. Mol. Biol.* **101**, 537-552 (1976).
9. Bergemann, K. & Nierhaus, K.H. Spontaneous, elongation factor G independent translocation of Escherichia coli ribosomes. *J. Biol. Chem.* **258**, 15105-15113 (1983).